Time dependence of the position momentum and position velocity uncertainties in gapped graphene

Eylee Jung,[1] Kwang S. Kim,[1] and DaeKil Park[2,3]

[1]*Center for Superfunctional Materials, Department of Chemistry, Pohang University of Science and Technology, San 31, Hyojadong, Namgu, Pohang 790-784, Korea*

[2]*Department of Physics, Kyungnam University, ChangWon, 631-701, Korea*

[3]*Department of Electronic Engineering, Kyungnam University, ChangWon, 631-701, Korea*

(Received 27 July 2011; published 9 April 2012)

We examine the time dependence of the position-momentum and position-velocity uncertainties in monolayer gapped graphene. The effect of the energy gap to the uncertainties is shown to appear via the Compton-like wavelength λ_c. The uncertainties in the graphene are mainly contributed by two phenomena, spreading and zitterbewegung. While the former determines the uncertainties in the long range of time, the latter gives high oscillation to the uncertainties in the short range of time. The uncertainties in the graphene are compared with the corresponding values for the usual free Hamiltonian $\hat{H}_{\text{free}} = (p_1^2 + p_2^2)/2M$. It is shown that the uncertainties can be under control within the quantum mechanical laws if one can choose the gap parameter λ_c freely.

DOI: 10.1103/PhysRevB.85.165418 PACS number(s): 73.22.−f, 03.65.Pm

I. INTRODUCTION

After success for fabricating the monolayer or few layer graphene,[1] there are a lot of activities for researching into the various properties of graphene.[2] This is mainly due to the fact that the low-energy electrons in graphene have unusual electronic properties.

Long ago it was predicted by Wallace[3] that the electron located near the hexagonal vertices of the Brillouin zone exhibits a linear dispersion relation and, 40 years later, Semenoff[4] showed that the low-energy dynamics of the corresponding electron is governed by a massless Dirac equation even in the nonrelativistic regime. Thus, the fabrication of the monolayer graphene opens a possibility to test various predictions of quantum electrodynamics (QED) by making use of condensed matter experiment. However, this does not mean that all phenomena QED predicted can be realized in the graphene-based experiment because the light velocity c in QED should be replaced by the Fermi velocity $v_F \sim c/300$. It results in the large fine-structure constant $\alpha \sim 2$. This implies that only nonperturbative characters of the planar QED can be realized in the graphene experiment. Recently, there has been much research directed at this connection.[5]

Among many phenomena arising in the planar QED, the most interesting issue, at least for us, is the spin-1/2 Aharonov-Bohm (AB)[6] or Aharonov-Bohm-Coulomb (ABC) problem, which was extensively discussed about two decades ago[7] because the same problem appeared in the context of anyonic and cosmic string theories.[8] The most important issue in this problem is how to treat the δ-like singular potential generated by an interaction between particle's spin and thin magnetic flux tube. Recently, similar AB and related problems were discussed theoretically[9] and experimentally[10] in the branch of graphene physics. Another closely related issue in the graphene is Coulomb impurity problem.[11] The interesting fact in this case is that, depending on the charge of impurity, there are two regions, the subcritical and supercritical, in which the effects of impurity differ completely. A similar phenomenon in QED was discussed long ago in Ref. 12.

Other unobserved interesting phenomena that QED predicts are the Klein paradox and zitterbewegung. The Klein paradox[13]-counterintuitive barrier penetration in the relativistic setting was re-examined in Ref. 14. The authors of Ref. 14 argued that the Klein paradox can be realized using electrostatic barriers in single- and bilayer graphene. A few years later it was reported that the Klein tunneling was observed by measuring the quantum conductance oscillation and phase-shift pattern in extremely narrow graphene.[15] The zitterbewegung (ZB),[16] the trembling motion arising due to the interference between positive and negative energy states, was also investigated recently in graphene without[17] and with[18] an external magnetic field. The effect of zitterbewegung for other models also has been discussed recently.[19]

In addition to a connection between graphene and QED, much attention has been paid to graphene as a new material for future technology. The most important application of graphene, at least for us, is the possibility for realization of a quantum computer. Recently, many techniques have been used independently or cooperatively to realize a quantum computer. The typical techniques are optical ones: ion traps, NMR, quantum dots, and superconductors. The current status for this realization is summarized in detail in Ref. 20. Also, the graphene-based quantum computer is explored in Ref. 21.

In this paper we will examine the position-momentum and position-velocity uncertainties of low-energy electrons in the monolayer gapped graphene when the initial wave packet is chosen as a general Gaussian wave packet. Since a Gaussian wave packet, in general, contains both positive-energy and negative-energy spectra, the expectation values of the physical quantities should be the result of spreading and zitterbewegung. Thus, it is of interest to examine the effect of the gap parameter in the expectation values of various quantities and uncertainties. We will show in this paper that the position-momentum and position-velocity uncertainties can be under control within the quantum-mechanical laws if the gap parameter can be chosen freely.

Although this controllability of the uncertainties is interesting on purely theoretical grounds, it is also important in terms of realizing a quantum computer. The quantum computer[20] is a machine that performs quantum computational processes by making use of quantum mechanical laws. So far, many quantum information processes have been developed, such as quantum teleportation,[22] factoring algorithm,s[23] and search algorithms.[24] All quantum information processes consist of three stages: preparation of initial states at the initial stage, time evolution of quantum states via various unitary gates at the intermediate stage, and quantum measurements at the final stages. If uncertainties, therefore, are large at the final stage, the quantum measurement can generate fatal errors in the computing processes. For this reason, it is important to reduce the uncertainties as much as possible at the final stages.

This paper is organized as follows. In Sec. II, we examine the position-momentum uncertainties in gapped graphene. It is shown that the uncertainties are the result of the spreading and ZB effects of the given wave packet. The uncertainties in the gapped graphene are compared with the corresponding quantities of the 2D free Hamiltonian system. In Sec. III, we discuss the position-velocity uncertainties in gapped graphene. Unlike the position uncertainties, the velocity uncertainties are shown to be solely the result of the ZB effect of the wave packet. This implies that the $t \to \infty$ limit of the velocity uncertainties coincides with the Fermi velocity v_F regardless of the choice of the packet. In Sec. IV, a brief conclusion is given.

II. POSITION-MOMENTUM UNCERTAINTY

In this section we examine the position-momentum uncertainty in gapped graphene. The appropriate Hamiltonian for the low-energy electron near the Dirac point is given by

$$\hat{H}_M = v_F \begin{pmatrix} M v_F & p_1 - i p_2 \\ p_1 + i p_2 & -M v_F \end{pmatrix}, \tag{1}$$

where $v_F \sim c/300$ is the Fermi velocity and M is a gap parameter generated for some dynamical and technical reasons. Theoretically, the most popular mechanism that generates the gap is chiral symmetry breaking.[25] This mechanism is similar to that of dynamical breaking,[26] which was studied deeply in gauge theories. The band gap can be generated by breaking the sublattice symmetry. This case was experimentally realized by choosing the substrate appropriately.[27] In addition, the gap is also generated in a graphene nanoribbon.[28] Both cases are taken into account in the Hamiltonian of Eq. (1). Although monolayer graphene itself does not have a gap, the band gap is naturally generated in bilayer graphene.[29] However, we cannot use the Hamiltonian of Eq. (1) to explore the effect of the gap in the bilayer graphene due to the nontrivial structure of the gap in the bilayer system. From the terminology of relativistic field theories, this gap parameter M is a mass term of the Dirac fermion.

The position operator $\hat{x}(t)$ in the Heisenberg picture can be expressed by a 2×2 matrix from $\hat{x}(t) = \exp(i\hat{H}_M t/\hbar)\hat{x}(0)\exp(-i\hat{H}_M t/\hbar)$. Explicit calculation shows

$$\hat{x}(t) = \hat{x}(0) + \begin{bmatrix} \hat{\Sigma}(p) & \hat{\sigma}_1(p) + i\hat{\sigma}_2(p) \\ \hat{\sigma}_1(p) - i\hat{\sigma}_2(p) & -\hat{\Sigma}(p) \end{bmatrix}, \tag{2}$$

where

$$\begin{aligned} \hat{\Sigma}(p) &= \frac{\hbar}{\boldsymbol{p}^2 + (M v_F)^2}\Bigg[p_2 \sin^2\theta_M + \frac{(M v_F) p_1}{\sqrt{\boldsymbol{p}^2 + (M v_F)^2}} \\ &\quad \times (\theta_M - \sin\theta_M \cos\theta_M)\Bigg], \\ \hat{\sigma}_1(p) &= \frac{\hbar}{[\boldsymbol{p}^2 + (M v_F)^2]^{3/2}}\big[\theta_M p_1^2 + \sin\theta_M \cos\theta_M \\ &\quad \times \{p_2^2 + (M v_F)^2\}\big], \\ \hat{\sigma}_2(p) &= \frac{\hbar}{[\boldsymbol{p}^2 + (M v_F)^2]^{3/2}}[p_1 p_2 (\sin\theta_M\cos\theta_M - \theta_M) \\ &\quad + (M v_F)\sqrt{\boldsymbol{p}^2 + (M v_F)^2}\sin^2\theta_M], \end{aligned} \tag{3}$$

and $\theta_M = (v_F t/\hbar)\sqrt{\boldsymbol{p}^2 + (M v_F)^2}$. Each operator in Eq. (3) consists of two types, one of which is responsible for ZB phenomena and the other for spreading of the wave packet.

In order to examine the uncertainty relations, we should introduce a wave packet. In this paper we introduce the usual two-dimensional Gaussian wave packet,

$$\begin{aligned} |\psi(x,y:0)\rangle &= \frac{d}{2\pi\sqrt{\pi}} \int d^2\boldsymbol{k} \exp\Bigg[-\frac{d^2}{2}(k_x - \alpha)^2 \\ &\quad - \frac{d^2}{2}(k_y - \beta)^2\Bigg] e^{i\boldsymbol{k}\cdot\boldsymbol{r}} \begin{pmatrix} a \\ b \end{pmatrix}, \end{aligned} \tag{4}$$

where real parameters a and b satisfy $a^2 + b^2 = 1$. It is easy to show that $|\psi(x,y:0)\rangle$ can be decomposed as

$$|\psi(x,y:0)\rangle = |\psi^p(x,y:0)\rangle + |\psi^n(x,y:0)\rangle, \tag{5}$$

where $|\psi^p(x,y:0)\rangle$ and $|\psi^n(x,y:0)\rangle$ are the positive-energy and negative-energy components of $|\psi(x,y:0)\rangle$, respectively. Using the Hamiltonian $\hat{H}_M$, it is easy to derive these components, and the explicit expressions are given by

$$\begin{aligned} &|\psi^p(x,y:0)\rangle \\ &= \frac{d}{4\pi\sqrt{\pi}} \int d^2\boldsymbol{k} \exp\left[-\frac{d^2}{2}(k_x - \alpha)^2 - \frac{d^2}{2}(k_y - \beta)^2\right] e^{i\boldsymbol{k}\cdot\boldsymbol{r}} \\ &\quad \times \frac{a k_+ + b\left(\sqrt{\boldsymbol{k}^2 + \lambda_c^{-2}} - \lambda_c^{-1}\right)}{k_+\sqrt{\boldsymbol{k}^2 + \lambda_c^{-2}}} \begin{pmatrix} \sqrt{\boldsymbol{k}^2 + \lambda_c^{-2}} + \lambda_c^{-1} \\ k_+ \end{pmatrix}, \\ &|\psi^n(x,y:0)\rangle \\ &= \frac{d}{4\pi\sqrt{\pi}} \int d^2\boldsymbol{k} \exp\left[-\frac{d^2}{2}(k_x - \alpha)^2 - \frac{d^2}{2}(k_y - \beta)^2\right] e^{i\boldsymbol{k}\cdot\boldsymbol{r}} \\ &\quad \times \frac{a k_+ - b\left(\sqrt{\boldsymbol{k}^2 + \lambda_c^{-2}} + \lambda_c^{-1}\right)}{k_+\sqrt{\boldsymbol{k}^2 + \lambda_c^{-2}}} \begin{pmatrix} \sqrt{\boldsymbol{k}^2 + \lambda_c^{-2}} - \lambda_c^{-1} \\ -k_+ \end{pmatrix}. \end{aligned} \tag{6}$$

In Eq. (6), $k_\pm = k_x \pm i k_y$ and $\lambda_c = \hbar/(M v_F)$. The parameter λ_c is a familiar quantity. In fact, this is a Compton wavelength if the Fermi velocity v_F is replaced with the velocity of light c. In this paper, we refer to λ_c as the Compton wavelength. Thus, the intensity for the positive-energy and negative-energy components are

$$\begin{aligned} P_+ &\equiv \langle\psi^p(x,y:0)|\psi^p(x,y:0)\rangle = \tfrac{1}{2} + \Delta P, \\ P_- &\equiv \langle\psi^n(x,y:0)|\psi^n(x,y:0)\rangle = \tfrac{1}{2} - \Delta P = 1 - P_+, \end{aligned} \tag{7}$$

where

$$\Delta P = \frac{d^2}{2\pi}\int d^2\boldsymbol{k}\exp[-d^2(k_x-\alpha)^2 - d(k_y-\beta)^2] \times \frac{\lambda_c^{-1}(a^2-b^2)+2abk_x}{\sqrt{\boldsymbol{k}^2+\lambda_c^{-2}}}. \tag{8}$$

If, therefore, $\alpha = 0$ with $a = b = 1/\sqrt{2}$, we get $P_+ = P_- = 1/2$. In this case, the expectation values of various operators are summarized in Appendix A. For arbitrary α and β, however, $P_\pm$ should be computed numerically. Since $|\psi(x,y:0)\rangle$ has both positive-energy and negative-energy components, the expectation value of various physical quantities should exhibit the trembling behavior due to the interference of these components as discussed in Ref. 16–19.

Using Eqs. (2) and (4) it is straightforward to show

$$\begin{aligned}\langle x\rangle(t) &\equiv \langle\psi(x,y:0)|\hat{x}(t)|\psi(x,y:0)\rangle\\ &= \frac{d^2}{\pi}\int d^2\boldsymbol{k}\exp[-d^2(k_x-\alpha)^2 - d^2(k_y-\beta)^2]\\ &\quad\times(X_S + X_{\mathrm{ZB}}),\end{aligned} \tag{9}$$

where

$$\begin{aligned}X_S &= \frac{(v_F t)}{\boldsymbol{k}^2+\lambda_c^{-2}}[(a^2-b^2)\lambda_c^{-1}k_x + 2abk_x^2],\\ X_{\mathrm{ZB}} &= \frac{a^2-b^2}{\boldsymbol{k}^2+\lambda_c^{-2}}\left[k_y\sin^2\theta - \frac{\lambda_c^{-1}k_x}{\sqrt{\boldsymbol{k}^2+\lambda_c^{-2}}}\sin\theta\cos\theta\right]\\ &\quad+\frac{2ab}{\left(\boldsymbol{k}^2+\lambda_c^{-2}\right)^{3/2}}\sin\theta\cos\theta\left(k_y^2+\lambda_c^{-2}\right),\end{aligned} \tag{10}$$

and $\theta = (v_F t)\sqrt{\boldsymbol{k}^2+\lambda_c^{-2}}$. As noted before, X_S and X_{ZB} are responsible for the spreading and trembling motion in the time evolution of the packet, respectively. It is worthwhile noting that the $\boldsymbol{k}$ integration in Eq. (9) can be performed explicitly by making use of the binomial expansion. Finally, then, $\langle x\rangle(t)$ is represented in terms of the Hermite polynomials. Instead of integral representation, however, $\langle x\rangle(t)$ has triple summations. The explicit expressions in terms of the Hermite polynomials for various expectation values derived in this paper are summarized in Appendix B.

A similar calculation procedure derives $\langle y\rangle(t)$ as

$$\begin{aligned}\langle y\rangle(t) &\equiv \langle\psi(x,y:0)|\hat{y}(t)|\psi(x,y:0)\rangle\\ &= \frac{d^2}{\pi}\int d^2\boldsymbol{k}\exp[-d^2(k_x-\alpha)^2 - d^2(k_y-\beta)^2]\\ &\quad\times(Y_S + Y_{\mathrm{ZB}}),\end{aligned} \tag{11}$$

where

$$\begin{aligned}Y_S &= \frac{(v_F t)}{\boldsymbol{k}^2+\lambda_c^{-2}}[(a^2-b^2)\lambda_c^{-1}k_y + 2abk_xk_y],\\ Y_{\mathrm{ZB}} &= \frac{\sin^2\theta}{\boldsymbol{k}^2+\lambda_c^{-2}}[-(a^2-b^2)k_x + 2ab\lambda_c^{-1}]\\ &\quad-\frac{\sin\theta\cos\theta}{(\boldsymbol{k}^2+\lambda_c^{-2})^{3/2}}[(a^2-b^2)\lambda_c^{-1}k_y + 2abk_xk_y].\end{aligned} \tag{12}$$

Of course, Y_S and Y_{ZB} represent the spreading and ZB motion of the wave packet in the y direction.

In order to confirm the validity of our calculation, we consider the case of zero gap ($\lambda_c^{-1}\to 0$), which was considered in Ref. 17. For simplicity, we choose $\alpha = 0$, $a = 1$, and $b = 0$. Then, $Y_S = 0$ and $Y_{\mathrm{ZB}} = -\sin^2\theta k_x/\mathbf{k}^2$, which makes $\langle y\rangle(t) = 0$ due to k_x integration. In this case, we also get $X_S = 0$ and $X_{\mathrm{ZB}} = \sin^2\theta k_y/\mathbf{k}^2$. Using $\int_0^{2\pi} d\theta\sin\theta e^{a\sin\theta} = 2\pi I_1(a)$, where $I_\nu(z)$ is a modified Bessel function, one can show directly,

$$\begin{aligned}\langle x\rangle(t) &= \frac{1}{2\beta}\left(1-e^{-\beta^2d^2}\right) - de^{-\beta^2d^2}\int_0^\infty dq e^{-q^2}\\ &\quad\times\cos\left(\frac{2v_F t}{d}q\right)I_1(2\beta dq),\end{aligned} \tag{13}$$

which exactly coincides with the second reference of Ref. 17.

Before we explore the uncertainty properties, it is interesting to examine the limiting behaviors of $\langle x\rangle(t)$ and $\langle y\rangle(t)$. In the $t\to 0$ limit some combinations of the spreading and the trembling motion become dominant and the limiting behaviors reduce to

$$\begin{aligned}&\lim_{t\to 0}\langle x\rangle(t) = 2ab(v_F t) + O[(v_F t)^2],\\ &\lim_{t\to 0}\langle y\rangle(t) = (v_F t)^2[-(a^2-b^2)\alpha + 2ab\lambda_c^{-1}] + O[(v_F t)^3].\end{aligned} \tag{14}$$

It is interesting to note that the $t\to 0$ limiting behaviors of $\langle x\rangle(t)$ and $\langle y\rangle(t)$ differ completely because their orders of $v_F t$ differ from each other. Furthermore, the dominant terms of $\langle x\rangle(t)$ come from the off-diagonal components of $\hat{x}(t)$ while those of $\langle y\rangle(t)$ are the result of all the components of $\hat{y}(t)$. In the $t\to\infty$ limit, the dominant terms in $\langle x\rangle(t)$ and $\langle y\rangle(t)$ result from the spreading terms and their expressions are as follows:

$$\begin{aligned}\lim_{t\to\infty}\langle x\rangle(t) &= \frac{d^2(v_F t)}{\pi}\left[(a^2-b^2)\lambda_c^{-1}J_{1,0} + 2abJ_{2,0}\right],\\ \lim_{t\to\infty}\langle y\rangle(t) &= \frac{d^2(v_F t)}{\pi}\left[(a^2-b^2)\lambda_c^{-1}J_{0,1} + 2abJ_{1,1}\right],\end{aligned} \tag{15}$$

where

$$J_{m,n} \equiv \int d^2\boldsymbol{k}\exp[-d^2(k_x-\alpha)^2 - d^2(k_y-\beta)^2]\frac{k_x^mk_y^n}{\boldsymbol{k}^2+\lambda_c^{-2}}. \tag{16}$$

In order to examine the position uncertainty $\Delta x(t)$ we should derive $\hat{x}^2(t)$, which reduces to

$$\begin{aligned}\hat{x}^2(t) &= \left[\hat{x}^2(0) + \hat{\Sigma}^2(p) + \hat{\sigma}_1^2(p) + \hat{\sigma}_2^2(p)\right]\mathbb{1}\\ &\quad+\{\hat{x}(0),\hat{x}(t)-\hat{x}(0)\},\end{aligned} \tag{17}$$

where $\{A,B\}\equiv AB + BA$. Since it is straightforward to show $\langle\psi(x,y:0)|\{\hat{x}(0),\hat{Z}(p)\}|\psi(x,y:0)\rangle = 0$ with $\hat{Z} = \hat{\Sigma}$, $\hat{\sigma}_1$, or $\hat{\sigma}_2$, one can show directly

$$\begin{aligned}\langle x^2\rangle(t) &= \frac{d^2}{2} + \frac{d^2}{\pi}\int d^2\boldsymbol{k}\exp[-d^2(k_x-\alpha)^2 - d^2(k_y-\beta)^2]\\ &\quad\times(\tilde{X}_S + \tilde{X}_{\mathrm{ZB}}),\end{aligned} \tag{18}$$

where

$$\tilde{X}_S = (v_F t)^2\frac{k_x^2}{\boldsymbol{k}^2+\lambda_c^{-2}} \qquad \tilde{X}_{\mathrm{ZB}} = \sin^2\theta\frac{k_y^2+\lambda_c^{-2}}{\left(\boldsymbol{k}^2+\lambda_c^{-2}\right)^2}. \tag{19}$$

A similar calculation shows

$$\langle y^2\rangle(t) = \frac{d^2}{2} + \frac{d^2}{\pi}\int d^2\boldsymbol{k}\exp[-d^2(k_x-\alpha)^2 - d^2(k_y-\beta)^2] \times (\tilde{Y}_S + \tilde{Y}_{\rm ZB}), \tag{20}$$

where $\tilde{Y}_S$ and $\tilde{Y}_{\rm ZB}$ are obtained from $\tilde{X}_S$ and $\tilde{X}_{\rm ZB}$ by interchanging k_x with k_y.

For the case of zero gap ($\lambda_c^{-1} \to o$) with $\alpha = 0$, $a = 1$, and $b = 0$, one can show straightforwardly,

$$\begin{aligned}\langle x^2\rangle(t) &= \frac{d^2}{2} + \frac{(v_F t)^2}{2\beta^2 d^2}(1-e^{-\beta^2 d^2}) + d^2 e^{-\beta^2 d^2}\int_0^\infty \frac{dq}{q^2}e^{-q^2} \\ &\quad \times \left[1-\cos\left(\frac{2v_F t}{d}q\right)\right]\left[q I_0(2\beta d q) - \frac{1}{2\beta d}I_1(2\beta d q)\right], \\ \langle y^2\rangle(t) &= \frac{d^2}{2} + (v_F t)^2\left[e^{-\beta^2 d^2/2}\left(\sin\frac{\beta^2 d^2}{2} + \cos\frac{\beta^2 d^2}{2}\right) - \frac{1}{2\beta^2 d^2}(1-e^{-\beta^2 d^2})\right] \\ &\quad + \frac{d}{2\beta}e^{-\beta^2 d^2}\int_0^\infty \frac{dq}{q^2}e^{-q^2}\left[1-\cos\left(\frac{2v_F t}{d}q\right)\right] \\ &\quad \times I_1(2\beta d q).\end{aligned} \tag{21}$$

Equations (13) and (21) can be used to compute the uncertainties Δx and Δy for the case of zero gap.

In the $t \to 0$ limit $\langle x^2\rangle(t)$ and $\langle y^2\rangle(t)$ exhibit similar behavior as

$$\lim_{t\to 0}\langle x^2\rangle(t) = \lim_{t\to 0}\langle y^2\rangle(t) = \frac{d^2}{2} + (v_F t)^2 + O[(v_F t)^3], \tag{22}$$

and the $t \to \infty$ limits of $\langle x^2\rangle(t)$ and $\langle y^2\rangle(t)$ reduce to

$$\begin{aligned}\lim_{t\to\infty}\langle x^2\rangle(t) &= \frac{d^2}{2} + \frac{d^2}{\pi}(v_F t)^2 J_{2,0} \\ \lim_{t\to\infty}\langle y^2\rangle(t) &= \frac{d^2}{2} + \frac{d^2}{\pi}(v_F t)^2 J_{0,2}.\end{aligned} \tag{23}$$

Since it is easy to show $\Delta p_x = \Delta p_y = \hbar/\sqrt{2}d$, we plot the time dependence of the dimensionless quantity $\Delta x \Delta p_x/\hbar$ in Fig. 1. In the figure we choose $a = 0.9$, $d = 8$ (nm),

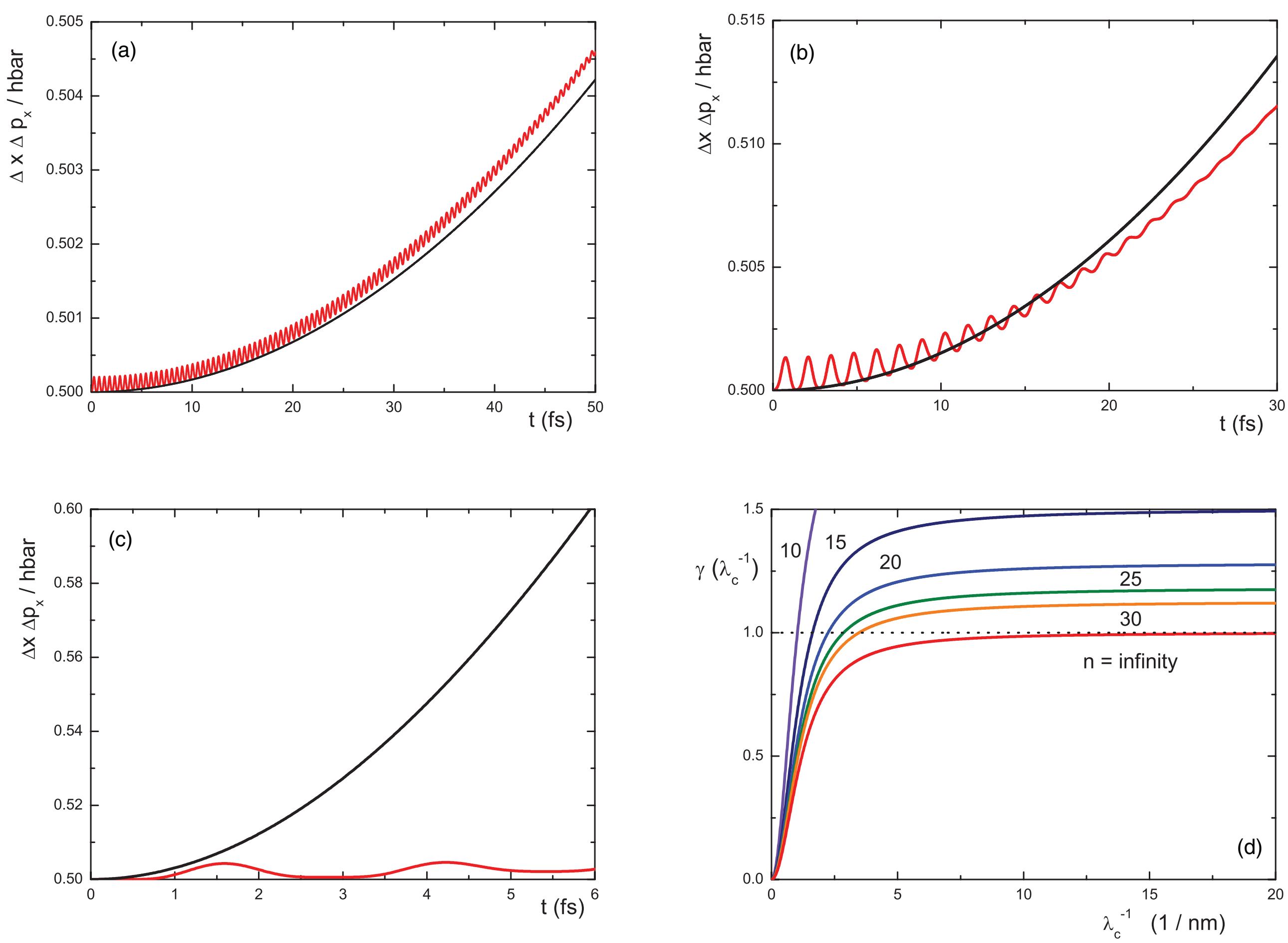

FIG. 1. (Color online) The time dependence of $\Delta x \Delta p_x/\hbar$ for $\lambda_c^{-1} = 6$ (1/nm) (a), $\lambda_c^{-1} = 2$ (1/nm) (b), and $\lambda_c^{-1} = 0.14$ (1/nm) (c). The black solid line for each figure is a corresponding value $(\Delta x \Delta p_x/\hbar)_{\rm free}$ for the usual two-dimensional free Hamiltonian $\hat{H}_{\rm free}$. As panels (a), (b), and (c) show, the uncertainty $\Delta x \Delta p_x$ in graphene is larger (or smaller) than $(\Delta x \Delta p_x)_{\rm free}$ in the entire range of time when $\lambda_c^{-1} > \mu_2$ (or $\lambda_c^{-1} < \mu_1$). When $\mu_1 < \lambda_c^{-1} < \mu_2$, $\Delta x \Delta p_x$ is larger and smaller than $(\Delta x \Delta p_x)_{\rm free}$ at $t \to 0$ and $t \to \infty$ limits, respectively. (d) The critical value μ_2 increases with decreasing α and eventually goes to ∞ at $\alpha = 0$.

$\alpha = 0.04$ (1/nm), and $\beta = 1.2$ (1/nm). We also choose the inverse of the Compton wave length as 6 (1/nm) [Fig. 1(a)], 2 (1/nm) [Fig. 1(b)], and 0.14 (1/nm) [Fig. 1(c)]. The black solid line in Figs. 1(a), 1(b), and 1(c) is $(\Delta x \Delta p_x/\hbar)_{\text{free}} = \sqrt{(1/2)^2 + (\lambda_c v_F t/2d^2)^2}$, which is a corresponding value for the usual nonrelativistic free Hamiltonian $\hat{H}_{\text{free}} = (p_1^2 + p_2^2)/2M$. The unit of the time axis is femtoseconds.

As Fig. 1 represents, the uncertainty $\Delta x \Delta p_x$ has several distinct properties. First, it is the result of both spreading and the ZB motion of the wave packet. The spreading motion dominates in the large scale of time. With an increase in the inverse Compton wavelength, the overall increasing rate of $\Delta x \Delta p_x$ resulting from spreading of the packet decreases drastically. This can be understood analogously from relativistic field theories, that is, specifically, the relativistic theory approach to the nonrelativistic Galilean theories, whereby, on increasing M, the uncertainty is minimized. In the small scale of time, $\Delta x \Delta p_x$ oscillates rapidly due to the ZB effect. The amplitude of the oscillation increases with decreasing λ_c^{-1}. This is mainly due to the fact the the ZB effect is dominated when the energy gap ΔE between positive and negative energy spectra decreases. However, the frequency increases rapidly with increasing λ_c^{-1} because of the famous formula $\omega = \Delta E/\hbar$. When λ_c^{-1} is larger than a critical value μ_2, $\Delta x \Delta p_x$ becomes larger than $(\Delta x \Delta p_x)_{\text{free}}$ as Fig. 1(a) indicates. When, however, λ_c^{-1} is smaller than a different critical value, μ_1, it is smaller than $(\Delta x \Delta p_x)_{\text{free}}$, as Fig. 1(c) shows. In the intermediate range of λ_c^{-1}, $\Delta x \Delta p_x$ is larger and smaller than $(\Delta x \Delta p_x)_{\text{free}}$ in the $t \to 0$ and $t \to \infty$ limits, respectively, as Fig. 1(b) shows. Using Eqs. (14) and (15) and several other limiting values, one can derive the critical values μ_1 explicitly, and μ_2 implicitly, as

$$\mu_1 = \frac{1}{\sqrt{2d^2(1-4a^2b^2)}}, \quad \gamma\left(\lambda_c^{-1}\right)\Big|_{\lambda_c^{-1}=\mu_2} = 1, \tag{24}$$

where

$$\gamma\left(\lambda_c^{-1}\right) = \frac{2\lambda_c^{-2}d^4}{\pi}\left[J_{2,0} - \frac{d^2}{\pi}\{(a^2-b^2)\lambda_c^{-1}J_{1,0} + 2abJ_{2,0}\}^2\right]. \tag{25}$$

The λ_c^{-1} dependence of $\gamma(\lambda_c^{-1})$ is plotted in Fig. 1(d), where $a = 0.9$, $d = 8$ (nm), $\alpha = 1.2/n$ (1/nm), and $\beta = 1.2$ (1/nm) for various n. As this figure indicates, the critical value μ_2

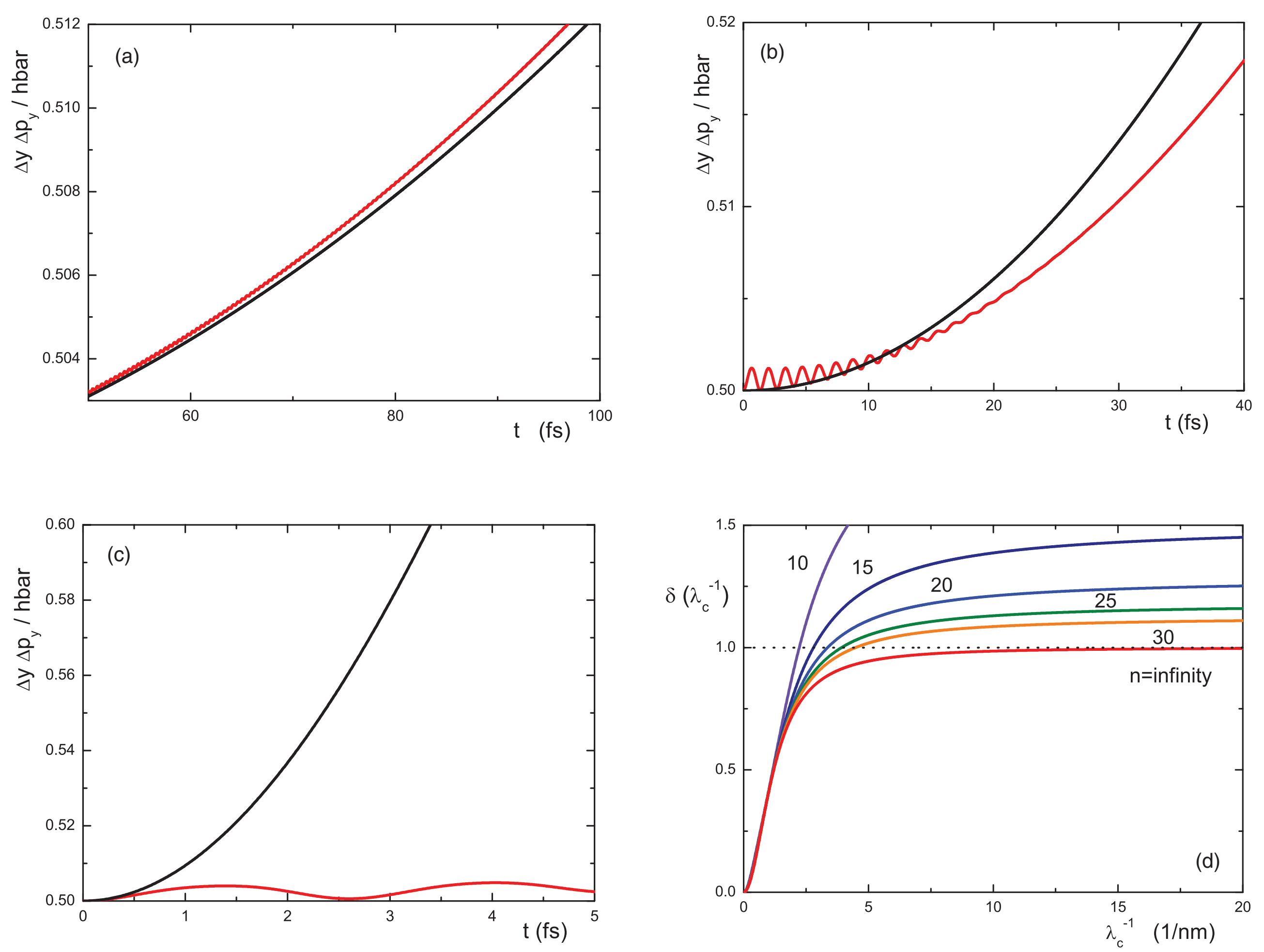

FIG. 2. (Color online) The time dependence of $\Delta y \Delta p_y/\hbar$ for $\lambda_c^{-1} = 8$ (1/nm) (a), $\lambda_c^{-1} = 2$ (1/nm) (b), and $\lambda_c^{-1} = 0.04$ (1/nm) (c). The black solid line for each figure is a corresponding value $(\Delta y \Delta p_y/\hbar)_{\text{free}}$. As panels (a), (b), and (c) show, the uncertainty $\Delta y \Delta p_y$ in graphene exhibits a similar behavior to $\Delta x \Delta p_x$. However, the critical values μ_1 and μ_2 are changed into ν_1 and ν_2. (d) The critical value ν_2 increases with decreasing β and eventually goes to ∞ at $\beta = 0$.

increases with increasing n, and, eventually, $\mu_2 = \infty$ when $\alpha = 0$.

The dimensionless uncertainty $\Delta y \Delta p_y/\hbar$ is plotted in Fig. 2, where $a = 0.9$, $d = 8$ (nm), $\alpha = 1.2$ (1/nm), and $\beta = 0.04$ (1/nm). We also choose λ_c^{-1} as 8 (1/nm) [Fig. 2(a)], 2 (1/nm) [Fig. 2(b)], and 0.08 (1/nm) [Fig. 2(c)]. We plot $(\Delta y \Delta p_y/\hbar)_{\text{free}}$ together for comparison. As Fig. 2 shows, $\Delta y \Delta p_y$ exhibits a similar behavior with $\Delta x \Delta p_x$. However, the critical values μ_1 and μ_2 are changed into ν_1 and ν_2, which reduce to

$$\nu_1 = \frac{1}{\sqrt{2}d}, \quad \delta\left(\lambda_c^{-1}\right)\Big|_{\lambda_c^{-1}=\mu_2} = 1, \tag{26}$$

where

$$\delta\left(\lambda_c^{-1}\right) = \frac{2\lambda_c^{-2}d^4}{\pi}\left[J_{0,2} - \frac{d^2}{\pi}\left\{(a^2 - b^2)\lambda_c^{-1}J_{0,1} + 2abJ_{1,1}\right\}^2\right]. \tag{27}$$

The λ_c^{-1} dependence of $\delta(\lambda_c^{-1})$ is plotted in Fig. 2(d), where $a = 0.9$, $d = 8$ (nm), $\alpha = 1.2$ (1/nm), and $\beta = 1.2/n$ (1/nm) for various n. As this figure indicates, the critical value ν_2 increases with increasing n and eventually goes to ∞ when $\beta = 0$.

III. POSITION-VELOCITY UNCERTAINTY

In this section we discuss the position-velocity uncertainties,[30] which differ completely from position-momentum uncertainties because of $\boldsymbol{p} \neq M\boldsymbol{v}$. The velocity operator $\hat{v}_x(t)$ is defined as $\exp(i\hat{H}_M t/\hbar)\hat{v}_x(0)\exp(-i\hat{H}_M t/\hbar)$, where $\hat{v}_x(0) = \partial\hat{H}_M/\partial p_1$. This operator is easily constructed from $\hat{x}(t)$ by making use of the Ehrenfest[31] theorem $d\hat{x}(t)/dt = (i/\hbar)\exp(i\hat{H}_M t/\hbar)[\hat{H}_M,\hat{x}(0)]\exp(-i\hat{H}_M t/\hbar) = \hat{v}_x(t)$. The final expression of $\hat{v}_x(t)$ then is

$$\hat{v}_x(t) = \begin{bmatrix} \hat{U}(p) & \hat{u}_1(p) + i\hat{u}_2(p) \\ \hat{u}_1(p) - i\hat{u}_2(p) & -\hat{U}(p) \end{bmatrix}, \tag{28}$$

where

$$\hat{U}(p) = v_F\left[\frac{2p_2}{\sqrt{\boldsymbol{p}^2 + (Mv_F)^2}}\sin\theta_M\cos\theta_M + \frac{2(Mv_F)p_1}{\boldsymbol{p}^2 + (Mv_F)^2}\sin^2\theta_M\right],$$

$$\hat{u}_1(p) = v_F\left[\cos^2\theta_M + \frac{p_1^2 - p_2^2 - (Mv_F)^2}{\boldsymbol{p}^2 + (Mv_F)^2}\sin^2\theta_M\right],$$

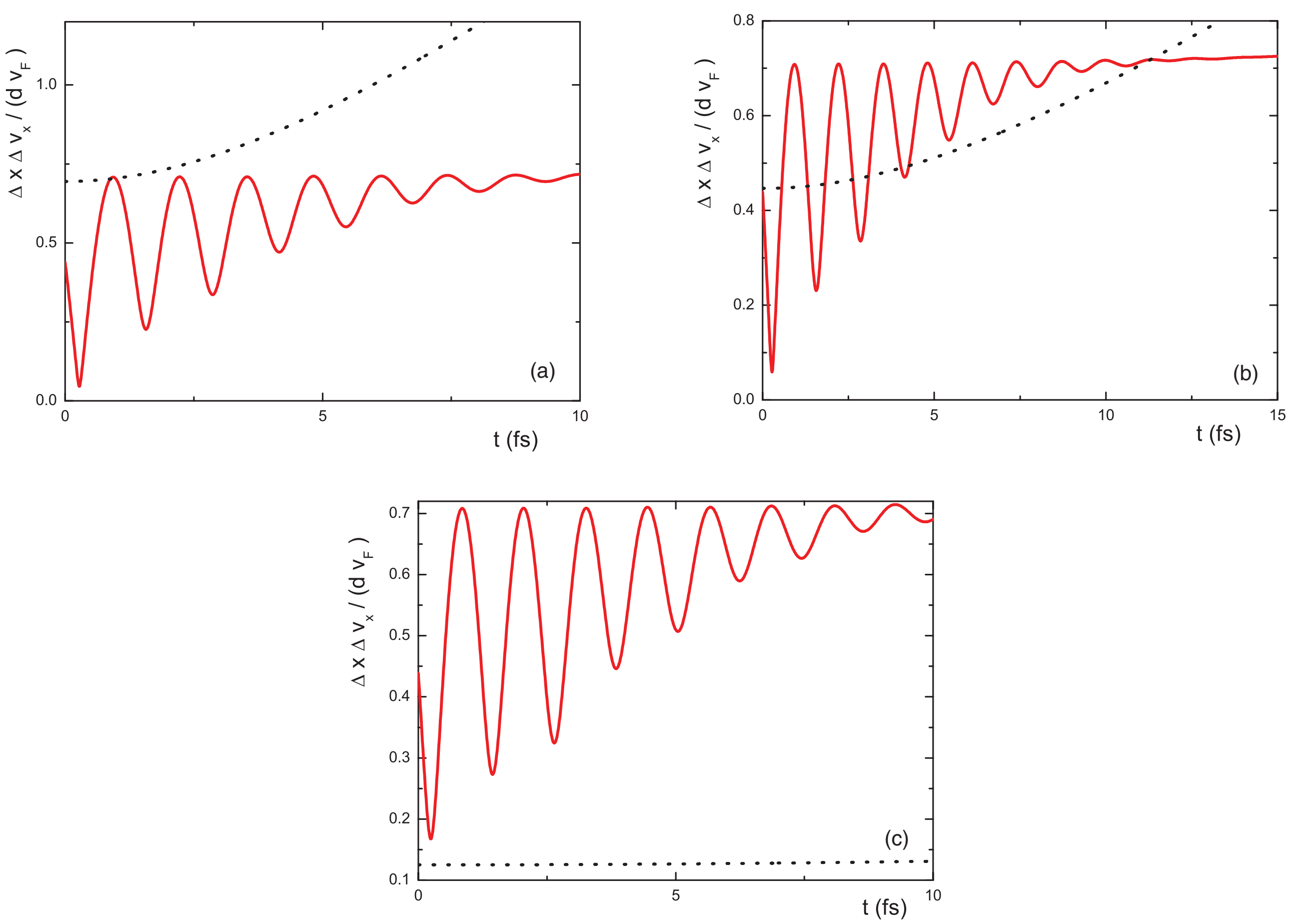

FIG. 3. (Color online) The time dependence of $\Delta x \Delta v_x/dv_F$ for $\lambda_c^{-1} = 0.09$ (1/nm) (a), $\lambda_c^{-1} = 0.14$ (1/nm) (b), and $\lambda_c^{-1} = 0.5$ (1/nm) (c). The black dotted line for each figure is a corresponding value for $(\Delta x \Delta v_x/dv_F)_{\text{free}}$. As panels (a), (b), and (c) show, the uncertainty $\Delta x \Delta v_x$ in graphene is larger (or smaller) than $(\Delta x \Delta v_x)_{\text{free}}$ depending on the gap parameter λ_c^{-1}. One can show explicitly that $\lim_{t\to 0}\Delta x \Delta v_x < (\Delta x \Delta v_x)_{\text{free}}$ if $\lambda_c^{-1} < \mu_1$ and $\lim_{t\to\infty}\Delta x \Delta v_x > (\Delta x \Delta v_x)_{\text{free}}$ if $\lambda_c^{-1} > \mu_{2*}$, where μ_{2*} is defined as $\gamma(\lambda_c^{-1} = \mu_{2*}) = 1/(2(\mu_{2*}d)^2)$.

TABLE I. Critical values for $\Delta x \Delta p_x$ and $\Delta x \Delta v_x$ when $d = 8$ (nm), $\alpha = 1.2/n$ (1/nm), and $\beta = 1.2$ (1/nm).

	a	$n = 10$	$n = 20$	$n = 30$	$n = 40$	$n = 50$	$n = \infty$
μ_1 (1/nm)	0.9	0.143	0.143	0.143	0.143	0.143	0.143
	0.7	4.42	4.42	4.42	4.42	4.42	4.42
μ_2 (1/nm)	0.9	1.03	2.24	3.47	4.69	5.90	∞
	0.7	0.90	1.79	2.68	3.58	4.47	∞
μ_{2*} (1/nm)	0.9	0.257	0.303	0.318	0.324	0.327	0.332
	0.7	0.256	0.302	0.317	0.323	0.326	0.332

$$\hat{u}_2(p) = v_F \left[-\frac{2 p_1 p_2}{\boldsymbol{p}^2 + (M v_F)^2} \sin^2 \theta_M + \frac{2(M v_F)}{\sqrt{\boldsymbol{p}^2 + (M v_F)^2}} \sin \theta_M \cos \theta_M \right]. \tag{29}$$

Unlike the position operators $\hat{x}(t)$ and $\hat{y}(t)$ the velocity operator $\hat{v}_x(t)$ does not have the spreading term. This is due to the fact that the spreading term in the position operators is linear in time. Another remarkable property of $\hat{v}_x(t)$ is that $\hat{v}_x^2(t)$ is simply v_F^2 times identity operator $\mathbb{1}$. Combining these two properties one can easily conjecture $\lim_{t\to\infty} \Delta v_x = v_F$ regardless of the choice of the wave packet because the ZB term in $\hat{v}_x(t)$ has infinitely high frequency in this limit and, therefore, is canceled out in the time average.

The expectation value $\langle v_x \rangle(t)$ and $\langle v_x^2 \rangle(t)$ with a wave packet (4) can be straightforwardly computed by making use of Eq. (28). As expected the resulting $\Delta v_x(t)$ has only trembling motion and approaches to v_F at $t \to \infty$ limit. The dimensionless position-velocity uncertainty $\Delta x \Delta v_x / d v_F$ is plotted in Fig. 3 for $\lambda_c^{-1} = 0.09$ (1/nm) [Fig. 3(a)], $\lambda_c^{-1} = 0.14$ (1/nm) [Fig. 3(b)], and $\lambda_c^{-1} = 0.5$ (1/nm) [Fig. 3(c)] when $a = 0.9$, $d = 8$ (nm), $\alpha = 0.04$ (1/nm), and $\beta = 1.2$ (1/nm). The x axis is the time axis with the unit in femtoseconds. The black dotted line is a corresponding value $(\Delta x \Delta v_x)_{\text{free}}/d v_F$, where $(\Delta x \Delta v_x)_{\text{free}} = \sqrt{\lambda_c^2 v_F^2/4 + \lambda_c^4 v_F^4 t^2/4d^4}$ is a position-velocity uncertainty for $\hat{H}_{\text{free}}$. The overall increasing behavior of $\Delta x \Delta v_x$ is solely due to Δx because Δv_x does not have its own spreading term. As Fig. 3 shows, $\Delta x \Delta v_x$ can be smaller or larger than $(\Delta x \Delta v_x)_{\text{free}}$ depending on the gap parameter λ_c. In order to compare $\Delta x \Delta v_x$ with $(\Delta x \Delta v_x)_{\text{free}}$ more accurately we compute its limiting values at $t \to 0$ and $t \to \infty$. It then is easy to show $\lim_{t\to 0} \Delta x \Delta v_x < (\Delta x \Delta v_x)_{\text{free}}$ if $\lambda_c^{-1} < \mu_1$, where μ_1 is defined at Eq. (24), and $\lim_{t\to\infty} \Delta x \Delta v_x > (\Delta x \Delta v_x)_{\text{free}}$ if $\lambda_c^{-1} > \mu_{2*}$, where μ_{2*} is defined as $\gamma(\lambda_c^{-1} = \mu_{2*}) = 1/(2(\mu_{2*} d)^2$. The critical values μ_1, μ_2, and μ_{2*} are given in Table I, where $d = 8$ (nm), $\alpha = 1.2/n$ (1/nm), $\beta = 1.2$ (1/nm), and $a = 0.9$ or 0.7. The reason for choosing a is that, while the diagonal components of the various operators contribute dominantly to the uncertainty relations at $a = 0.9 \sim 1$, the off-diagonal components become more important at $a = 0.7 \sim 1/\sqrt{2}$. As expected from Fig. 1(d), μ_2 increases with increasing n and eventually goes to ∞ at $\alpha = 0$. Another critical value μ_{2*} also exhibits an increasing behavior with increasing n, but its increasing rate is very small compared to μ_2 and converges to 0.332 at the $n \to \infty$ limit.

TABLE II. Critical values for $\Delta y \Delta p_y$ and $\Delta y \Delta v_y$ when $d = 8$ (nm), $\alpha = 1.2$ (1/nm), and $\beta = 1.2/n$ (1/nm).

	a	$n = 10$	$n = 20$	$n = 30$	$n = 40$	$n = 50$	$n = \infty$
ν_1 (1/nm)	0.9	0.088	0.088	0.088	0.088	0.088	0.088
	0.7	0.088	0.088	0.088	0.088	0.088	0.088
ν_2 (1/nm)	0.9	2.23	3.36	4.48	5.60	6.73	∞
	0.7	1.22	2.05	2.88	3.73	4.59	∞
ν_{2*} (1/nm)	0.9	0.309	0.326	0.329	0.330	0.331	0.332
	0.7	0.319	0.328	0.330	0.331	0.331	0.332

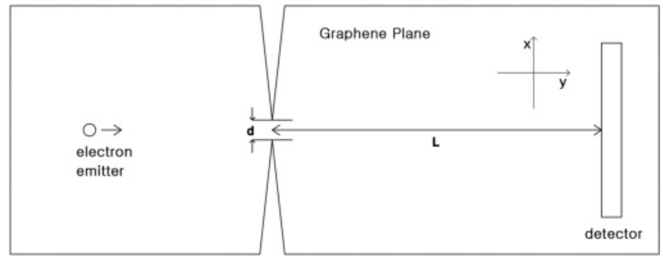

FIG. 4. Schematic diagram for measuring uncertainties.

Following a similar calculation procedure, one can plot the time dependence of the dimensionless quantity $\Delta y \Delta v_y/(d v_F)$. Although the time dependence of the uncertainties is not plotted in this paper, $\Delta y \Delta v_y$ exhibits a similar behavior with $\Delta x \Delta v_x$. However, the critical values μ_1 and μ_{2*} are changed into ν_1 and ν_{2*}, whose explicit values are given in Table II.

IV. CONCLUDING REMARKS

In this paper we have examined the position-momentum and position-velocity uncertainties for monolayer gapped graphene. We have shown that the uncertainties result from the spreading effect of the wave packet in the long range of time and the ZB in the short range of time. By choosing the gap parameter λ_c appropriately, one can control the uncertainties within quantum mechanical law.

The uncertainties can be tested experimentally because all figures in this paper show a significant difference between the free and graphene cases. The uncertainties in graphene might be measured via the following one-slit experiment (see Fig. 4). In this paper, we will discuss on Δx only because other quantities can be measured similarly. The slit width d should be in angstroms to ensure the occurrence of diffraction in the slit. The distance L should be in nanometers because the effect of the zitterbewegung is important within the initial few femtoseconds. The electrons emitted by the emitter would arrive at the detecter through the slit. One then can make a probability distribution with respect to x, which would be a smooth Gaussian form. Measuring the width of the Gaussian distribution, one can deduce Δx at $t \sim L/v_F$, where v_F is a Fermi velocity. Repeating the same experiment with changing L, one can measure the time dependence of Δx. If the prediction presented in this paper is correct, Δx would exhibit an oscillating behavior in the short range of time due to the effect of the zitterbewegung but, globally, an increasing behavior in the long range of time due to the spreading effect of the wave packet.

It would be interesting to extend the approach used in this paper to bilayer graphene. Another interesting issue would be to examine the uncertainty relations when an external magnetic field is applied. We hypothesize that the external magnetic field would drastically reduce the uncertainties in the graphene. If so, the graphene-based quantum computer could be more useful for huge calculations. We would like to explore this issue in the near future.

ACKNOWLEDGMENT

This research was supported by the Basic Science Research Program through the National Research Foundation of Korea (NRF) funded by the Ministry of Education, Science and Technology (Grant No. 2011-0011971) and the National Scientist Program (Grant No. 2010-0020414).

APPENDIX A

In this appendix we summarize the various expectation values at $\alpha = 0$ and $a = b = 1/\sqrt{2}$, where Eqs. (7) and (8) imply that the initial wave packet has equal intensity of positive-energy and negative-energy states. In this simple case the expectation values $\langle x\rangle(t)$ and $\langle y\rangle(t)$ reduce to

$$\langle x\rangle(t) = \frac{d^2}{\pi}\int d^2\mathbf{k} e^{-d^2k_x^2-d^2(k_y-\beta)^2} \times \left[(v_F t)\frac{k_x^2}{\mathbf{k}^2+\lambda_c^{-2}} + \sin\theta\cos\theta\frac{k_y^2+\lambda_c^{-2}}{\left(\mathbf{k}^2+\lambda_c^{-2}\right)^{3/2}}\right],$$
$$\langle y\rangle(t) = \frac{d^2\lambda_c^{-1}}{\pi}\int d^2\mathbf{k} e^{-d^2k_x^2-d^2(k_y-\beta)^2}\frac{\sin^2\theta}{\mathbf{k}^2+\lambda_c^{-2}}, \tag{A1}$$

where $\theta = (v_F t)\sqrt{\mathbf{k}^2+\lambda_c^{-2}}$. In the case of zero gap we get $\langle y\rangle(t) = 0$. Since $\langle x^2\rangle(t)$ and $\langle y^2\rangle(t)$ are independent of choice of a and b, they are equal to Eqs. (18) and (20) with $\alpha = 0$. The expectation values for the velocity operators becomes

$$\langle v_x\rangle(t) = v_F - \frac{2v_F d^2}{\pi}\int d^2\mathbf{k} e^{-d^2k_x^2-d^2(k_y-\beta)^2}\sin^2\theta\frac{k_y^2+\lambda_c^{-2}}{\mathbf{k}^2+\lambda_c^{-2}},$$
$$\langle v_y\rangle(t) = \frac{v_F d^2\lambda_c^{-1}}{\pi}\int d^2\mathbf{k} e^{-d^2k_x^2-d^2(k_y-\beta)^2}\frac{\sin 2\theta}{\sqrt{\mathbf{k}^2+\lambda_c^{-2}}}. \tag{A2}$$

In the case of zero gap we also get $\langle v_y\rangle(t) = 0$. Of course, the expectation values for the square of velocity operators are simply $\langle v_x^2\rangle = \langle v_y^2\rangle = v_F^2$.

APPENDIX B

In this appendix we summarize the explicit expressions for $\langle x\rangle(t)$, $\langle y\rangle(t)$, $\langle x^2\rangle(t)$, $\langle y^2\rangle(t)$, $\langle v_x\rangle(t)$, and $\langle v_y\rangle(t)$ by making use of the binomial expansion and performing the **k** integration. The integral formula we use is

$$\int_{-\infty}^{\infty} x^n e^{-(x-\beta)^2}dx = (2i)^{-n}\sqrt{\pi}H_n(i\beta), \tag{B1}$$

where $H_n(z)$ is the usual Hermite polynomial.

The expectation values $\langle x\rangle(t)$ and $\langle y\rangle(t)$, expressed in Eqs. (9) and (11), reduce to

$$\langle x\rangle(t) = 2abv_F t + \sum_{n=0}^{\infty}\frac{\left(2\lambda_c^{-1}v_F t\right)^{2n+2}}{(2n+3)!}\sum_{\ell=0}^{n}\binom{n}{\ell}\frac{(-1)^{n-\ell}}{\left(2\lambda_c^{-1}d\right)^{2\ell+2}} \times \sum_{m=0}^{\ell}\binom{\ell}{m}[-i(a^2-b^2)dX_1 + 2ab(v_F t)X_2],$$
$$\langle y\rangle(t) = \sum_{n=0}^{\infty}\frac{\left(2\lambda_c^{-1}v_F t\right)^{2n+2}}{(2n+3)!}\sum_{\ell=0}^{n}\binom{n}{\ell}\frac{(-1)^{n-\ell}}{\left(2\lambda_c^{-1}d\right)^{2\ell+2}} \times \sum_{m=0}^{\ell}\binom{\ell}{m}[i(a^2-b^2)dY_1 + ab\lambda_c Y_2], \tag{B2}$$

where

$$\begin{aligned}
X_1 &= (2n+3)H_{2m}(i\alpha d)H_{2\ell-2m+1}(i\beta d) + 2\left(\lambda_c^{-1}v_F t\right)H_{2m+1}(i\alpha d)H_{2\ell-2m}(i\beta d),\\
X_2 &= H_{2m}(i\alpha d)H_{2\ell-2m+2}(i\beta d) - \left(2\lambda_c^{-1}d\right)^2 H_{2m}(i\alpha d)H_{2\ell-2m}(i\beta d),\\
Y_1 &= (2n+3)H_{2m+1}(i\alpha d)H_{2\ell-2m}(i\beta d) + 2\left(\lambda_c^{-1}v_F t\right)H_{2m}(i\alpha d)H_{2\ell-2m+1}(i\beta d),\\
Y_2 &= (2n+3)\left(2\lambda_c^{-1}d\right)^2 H_{2m}(i\alpha d)H_{2\ell-2m}(i\beta d) - 2\left(\lambda_c^{-1}v_F t\right)H_{2m+1}(i\alpha d)H_{2\ell-2m+1}(i\beta d).
\end{aligned} \tag{B3}$$

Although the arguments of the Hermite polynomials are purely imaginary, one can show easily that $\langle x\rangle(t)$ and $\langle y\rangle(t)$ are real by considering the fact that $H_n(z)$ is an even (or odd) function when n is even (or odd).

Similarly, one can express $\langle x^2\rangle(t)$ and $\langle y^2\rangle(t)$ from Eqs. (18) and (20) as follows:

$$\langle x^2\rangle(t) = \frac{d^2}{2} + (v_F t)^2 + 2d^2\sum_{n=0}^{\infty}\frac{\left(2\lambda_c^{-1}v_F t\right)^{2n+4}}{(2n+4)!} \times \sum_{\ell=0}^{n}\binom{n}{\ell}\frac{(-1)^{n-\ell}}{\left(2\lambda_c^{-1}d\right)^{2\ell+4}}\sum_{m=0}^{\ell}\binom{\ell}{m}X_3,$$
$$\langle y^2\rangle(t) = \frac{d^2}{2} + (v_F t)^2 + 2d^2\sum_{n=0}^{\infty}\frac{\left(2\lambda_c^{-1}v_F t\right)^{2n+4}}{(2n+4)!}\sum_{\ell=0}^{n}\binom{n}{\ell}\frac{(-1)^{n-\ell}}{\left(2\lambda_c^{-1}d\right)^{2\ell+4}} \times \sum_{m=0}^{\ell}\binom{\ell}{m}Y_3, \tag{B4}$$

where $X_3 = X_2$ and

$$Y_3 = H_{2m+2}(i\alpha d)H_{2\ell-2m}(i\beta d) - \left(2\lambda_c^{-1}d\right)^2 H_{2m}(i\alpha d) \times H_{2\ell-2m}(i\beta d). \tag{B5}$$

Although we have not derived the integral representations of $\langle v_x\rangle(t)$ and $\langle v_y\rangle(t)$ explicitly in the main text, their derivations are straightforward. The expressions of $\langle v_x\rangle(t)$ and $\langle v_y\rangle(t)$ in terms of the Hermite polynomials then are

$$\begin{aligned}\langle v_x\rangle(t) &= 2abv_F - 2v_F\sum_{n=0}^{\infty}\frac{\left(2\lambda_c^{-1}v_Ft\right)^{2n+1}}{(2n+2)!}\\ &\quad\times\sum_{\ell=0}^{n}\binom{n}{\ell}\frac{(-1)^{n-\ell}}{\left(2\lambda_c^{-1}d\right)^{2\ell+2}}\sum_{m=0}^{\ell}\binom{\ell}{m}\\ &\quad\times\left[i(a^2-b^2)\left(2\lambda_c^{-1}d\right)U_1+2ab\left(\lambda_c^{-1}v_Ft\right)U_2\right],\\ \langle v_y\rangle(t) &= v_F\sum_{n=0}^{\infty}\frac{\left(2\lambda_c^{-1}v_Ft\right)^{2n+1}}{(2n+2)!}\sum_{\ell=0}^{n}\binom{n}{\ell}\\ &\quad\times\frac{(-1)^{n-\ell}}{\left(2\lambda_c^{-1}d\right)^{2\ell+1}}\sum_{m=0}^{\ell}\binom{\ell}{m}[i(a^2-b^2)V_1+2abV_2],\end{aligned} \tag{B6}$$

where

$$\begin{aligned}U_1 &= (n+1)H_{2m}(i\alpha d)H_{2\ell-2m+1}(i\beta d)\\ &\quad+\left(\lambda_c^{-1}v_Ft\right)H_{2m+1}(i\alpha d)H_{2\ell-2m}(i\beta d),\\ U_2 &= \left(2\lambda_c^{-1}d\right)^2H_{2m}(i\alpha d)H_{2\ell-2m}(i\beta d)\\ &\quad-H_{2m}(i\alpha d)H_{2\ell-2m+2}(i\beta d),\\ V_1 &= (2n+2)H_{2m+1}(i\alpha d)H_{2\ell-2m}(i\beta d)\\ &\quad-2\left(\lambda_c^{-1}v_Ft\right)H_{2m}(i\alpha d)H_{2\ell-2m+1}(i\beta d),\\ V_2 &= (2n+2)\left(2\lambda_c^{-1}d\right)H_{2m}(i\alpha d)H_{2\ell-2m}(i\beta d)\\ &\quad-\frac{v_Ft}{d}H_{2m+1}(i\alpha d)H_{2\ell-2m+1}(i\beta d).\end{aligned} \tag{B7}$$

---

[1]K. Novoselov *et al.*, Nature (London) **438**, 197 (2005); K. S. Kim *et al.*, Nature **457**, 706 (2009); S. Bae *et al.*, Nat. Nanotechnol. **5**, 574 (2010).

[2]For a recent review, see A. H. Castro Neto, F. Guinea, N. M. R. Peres, K. S. Novoselov, and A. K. Geim, Rev. Mod. Phys. **81**, 109 (2009) and references therein.

[3]P. R. Wallace, Phys. Rev. **71**, 622 (1947).

[4]G. W. Semenoff, Phys. Rev. Lett. **53**, 2449 (1984).

[5]R. Jackiw and S.-Y. Pi, Phys. Rev. Lett. **98**, 266402 (2007); J. K. Pachos and M. Stone, Int. J. Mod. Phys. B **21**, 5113 (2007); D. Allor, T. D. Cohen, and D. A. McGady, Phys. Rev. D **78**, 096009 (2008); C. G. Beneventano and E. M. Santangelo, J. Phys. A **41**, 164035 (2008); R. Jackiw and S.-Y. Pi, e-print arXiv:0808.1562 (cond-mat); E. M. Santangelo, e-print arXiv:0809.4844 (hep-th); C. G. Beneventano, P. Giacconi, E. M. Santangelo, and R. Soldati, J. Phys. A **42**, 275401 (2009); M. Bordag, I. V. Fialkovsky, D. M. Gitman, and D. V. Vassilevich, Phys. Rev. B **80**, 245406 (2009); G. W. Semenoff, e-print arXiv:1005.0572 (hep-th); A. Iorio, Ann. Phys. **326**, 1334 (2011); L. B. Drissi, E. H. Saidi, and M. Bousmina, Nucl. Phys. B **829**, 523 (2010).

[6]Y. Aharonov and D. Bohm, Phys. Rev. **115**, 485 (1959).

[7]R. Jackiw, in *M. A. B. Beg Memorial Volume*, edited by A. Ali and P. Hoodbhoy (World Scientific, Singapore, 1991); P. de Sousa Gerbert, Phys. Rev. D **40**, 1346 (1989); C. R. Hagen, Phys. Rev. Lett. **64**, 503 (1990); D. K. Park, J. Math. Phys. **36**, 5453 (1995); D. K. Park and S.-K. Yoo, Ann. Phys. **263**, 295 (1998).

[8]M. G. Alford and F. Wilczek, Phys. Rev. Lett. **62**, 1071 (1989); M. G. Alford, J. March-Russell, and F. Wilczek, Nucl. Phys. B **328**, 140 (1989); Y. H. Chen, F. Wilczek, E. Witten, and B. I. Halperin, Int. J. Mod. Phys. B **3**, 1001 (1989).

[9]P. Recher, B. Trauzettel, A. Rycerz, Y. M. Blanter, C. W. J. Beenakker, and A. F. Morpurgo, Phys. Rev. B **76**, 235404 (2007); A. Rycerz, Acta Phys. Pol. A **115**, 322 (1009); J. Wurm, M. Wimmer, H. U. Baranger, and K. Richter, Semicond. Sci. Technol. **25**, 034003 (2010); A. Rycerz and C. W. J. Beenakker, e-print arXiv:0709.3397 (cond-mat); R. Jackiw, A. I. Milstein, S.-Y. Pi, and I. S. Terekhov, Phys. Rev. B **80**, 033413 (2009); M. I. Katsnelson, Europhys. Lett. **89**, 17001 (2010); J. Schelter, D. Bohr, and B. Trauzettel, Phys. Rev. B **81**, 195441 (2010).

[10]S. Russo, J. B. Oostinga, D. Wehenkel, H. B. Heersche, S. S. Sobhani, L. M. K. Vandersypen, and A. F. Morpurgo, Phys. Rev. B **77**, 085413 (2008); F. Molitor *et al.*, New J. Phys. **12**, 043054 (2010).

[11]V. M. Pereira, J. Nilsson, and A. H. Castro Neto, Phys. Rev. Lett. **99**, 166802 (2007); A. V. Shytov, M. I. Katsnelson, and L. S. Levitov, *ibid.* **99**, 236801 (2007); **99**, 246802 (2007); V. M. Pereira, V. N. Kotov, and A. H. Castro Neto, Phys. Rev. B **78**, 085101 (2008); J. Wang, H. A. Fertig, and G. Murthy, Phys. Rev. Lett. **104**, 186401 (2010); F. de Juan, A. G. Grushin, and M. A. H. Vozmediano, Phys. Rev. B **82**, 125409 (2010).

[12]Y. B. Zeldovich and V. S. Popov, Sov. Phys. Usp. **14**, 673 (1972).

[13]O. Klein, Z. Phys. **53**, 157 (1929); N. Dombey and A. Calogeracos, Phys. Rep. **315**, 41 (1999).

[14]M. I. Katsnelson, K. Novoselov, and A. K. Geim, Nature (London) **2**, 620 (2006).

[15]A. F. Young and P. Kim, Nat. Phys. **5**, 222 (2009).

[16]J. D. Bjorken and S. D. Drell, *Relativistic Quantum Mechanics* (McGraw-Hill, New York, 1964).

[17]T. M. Rusin and W. Zawadzki, Phys. Rev. B **76**, 195439 (2007); J. Schliemann, New J. Phys. **10**, 043024 (2008); G. M. Maksimova, V. Ya. Demikhovskii, and E. V. Frolova, Phys. Rev. B **78**, 235321 (2008).

[18]T. M. Rusin and W. Zawadzki, Phys. Rev. B **78**, 125419 (2008); E. Romera and F. de los Santos, *ibid.* **80**, 165416 (2009); W. Zawadzki and T. M. Rusin, J. Phys.: Condens. Matter **23**, 143201 (2011).

[19]V. Ya. Demikhovskii, G. M. Maksimova, and E. V. Frolova, e-print arXiv:0912.0331 (cond-mat); V. Ya. Demikhovskii, G. M. Maksimova, A. A. Perov, and E. V. Frolova, e-print arXiv:1007.1566 (quant-ph).

[20]T. D. Ladd *et al.*, Nature **464**, 45 (2010), and references therein.

[21]B. Trauzettel, D. V. Bulaev, D. Loss, and G. Burkard, Nat. Phys. **3**, 192 (2007); P. Recher, J. Nilsson, G. Burkard, and B. Trauzettel, Phys. Rev. B **79**, 085407 (2009); P. Recher and B. Trauzettel, Nanotechnology **21**, 302001 (2010); T. Dirks *et al.*,

Nat. Phys. **7**, 386 (2011); G. Y. Wu, N.-Y. Lue, and L. Chang, e-print arXiv:1104.0443 (cond-mat).

[22] C. H. Bennett, G. Brassard, C. Crepeau, R. Jozsa, A. Peres, and W. K. Wootters, Phys. Rev. Lett. **70**, 1895 (1993).

[23] P. W. Shor, *Proc. 35th Annu. Symp. Foundation of Computer*, edited by S. Goldwasser (IEEE Comp. Soc. Press, Los Alamitos, CA, 1994).

[24] L. K. Grover, Phys. Rev. Lett. **79**, 325 (1997).

[25] Y. Araki and T. Hatsuda, Phys. Rev. B **82**, 121403(R) (2010).

[26] E. Farhi and R. Jackiw, *Dynamical Gauge Symmetry Breaking* (World Scientific, Singapore, 1982).

[27] S. Y. Zhou *et al.*, Nat. Mater. **6**, 770 (2007).

[28] M. Y. Han, B. Özyilmaz, Y. Zhang, and P. Kim, Phys. Rev. Lett. **98**, 206805 (2007); W. Y. Kim and K. S. Kim, Nat. Nanotechnol. **3**, 408 (2008).

[29] E. McCann and V. I. Fal'ko, Phys. Rev. Lett. **96**, 086805 (2006).

[30] M. H. Al-Hashimi and U.-J. Wiese, e-print arXiv:0907.5178 (quant-ph).

[31] L. L. Schiff, *Quantum Mechanics* (McGraw-Hill, Tokyo, 1968).